Comprehensive quantum chemical study of the associative complex of para-aminobenzoic acid and 7-diethylamino 4-methyl coumarin by adsorption and aromatic bridges

Shradha Lakhera
   Uttarakhand Open University

Kamal Devlal
   Uttarakhand Open University

Meenakshi Rana (✉ mrana@uou.ac.in)
   Uttarakhand Open University

Research Article

Abstract

The present study accounts for the quantum chemical and nonlinear optical properties of the combination of *para*-aminobenzoic acid and 7-diethylamino 4-methyl coumarin. Three different complexes were designed, surface interaction (adsorption) and two by connecting both molecules with π-bridge benzene and biphenyl. The amino and carboxyl groups were observed to behave as strong donor and acceptor sites in all the complexes. The band gap of the adsorbed complex was found more suitable. The absorption wavelength and intensity both were seen to increase with the increase in the number of benzene rings in the π-bridge. The chemical reactivity was established by the global reactivity descriptors. The values of first and second-order hyperpolarizability suggest the improved nonlinear optical responses of the introduced complexes. Additionally, the negative value of second-order hyperpolarizability suggests the possibility of the occurrence of reverse saturable absorption in these combinations. The reported work gives theoretical insights into the nonlinear optical properties of the combination of *para*-aminobenzoic acid and 7-diethylamino 4-methyl coumarin.

1. Introduction

Over the last few decades, considerable efforts have been made in designing and synthesizing new organic systems with large nonlinear optical (NLO) susceptibilities [1]. The laser-induced organic substances have significant nonlinear responses that possess the high responsive time, damage threshold, and hyperpolarizabilities, and have strong applications in the fields of optical limiting, telecommunications, optical computing, microfabrication, data storage, etc [2−4]. A number of researchers have introduced a new way to modify the charge transport properties and increase the nonlinear behavior of the compounds. Organic compounds bonded with the π-bridges (sometimes called chromophores, push-pull chromophores, or donor-π-acceptor chromophores) were seen to significantly enhance the nonlinear responses [5, 6]. Generally, the involvement of the benzene rings in the chromophores was found to be the main reason behind the increased nonlinear interactions with light [7]. The resonating structure of benzene causes an increment in the nonlinear abilities [8]. The conjugated single-double bond of the aromatic rings causes the interaction of two π-bonds or between a π-bond and a lone pair of electrons [9]. The delocalization of π-electrons mainly results in the increased dipole strength and polarizing ability of the compounds [10]. The high static dielectric constant of the benzene (2.274) can also be considered one more reason for the increased nonlinear responses [11]. A higher dielectric constant leads to an increased number of interfaces in the target compound which leads to increased anisotropic behavior of the compound [12]. The anisotropy is also relatable to the non-centrosymmetry as well as the hyperpolarizability of the compounds [13]. In simple words, we can say that a higher dielectric constant will lead to higher anisotropy, and an increase in the anisotropic nature leads to an increment in the polarizing ability of any compound [14].

Numerous research were seen in the literature where donor and acceptor compounds were seen to be connected with these π-bridges and the resultant structures were further used for several NLO applications like laser limiting, photo-switchable property, photo-luminescence quenching, and many

more [15, 16]. T.P. Gerasimova has done similar kind of work for the development of several donors-π-acceptor bridges using quinoxaline, quinoxalinone, quinoline, benzothiazole, and thiophene carboxaldehyde and worked on the halochroism properties of these chromophores [17]. The study on the chromophore formed by joining carbazole with a π-spacer group cyano ethynyl ethene designed by R. Kumar was successful in attaining huge first-order hyperpolarizability of 923.93×10^{-30} esu [18]. Novel V-shaped donor- π-acceptor chromophores 4-(1-Piperidinyl)benzaldehyde and 4-ethoxybenzaldehyde were designed and synthesized by Y. C. Feng et.al [19]. Further, the synthesized solutions were employed for investigating the possible two-photon absorption and also used for imaging purposes in living cells [19].

The present study is the future scope of our previously done experimental and computational studies on the NLO responses and optical limiting activity of para-aminobenzoic acid and 7-diethylamino 4-methyl coumarin (PABA and 7DMC) [20, 21]. The present study accounts for the computational predictions of the NLO responses of the combination of PABA and 7DMC. Structural, spectral, and reactivity calculations were performed for three different designed complex PABA and 7DMC, i.e., PABA + 7DMC complex **(1)**, PABA bonded with 7DMC with benzene **(2)**, and PABA bonded with 7DMC with a biphenyl **(3)**. Benzene and biphenyl were used as π-conjugated bridges and were used in numerous studies to connect π-bridges.

2. Materials and methods

The quantum chemical calculations reported in the present paper were done using density functional theory with the help of Gaussian (https://gaussian.com/) and Gauss View (https://gaussian.com/gaussview6/) software packages [22, 23]. The most generalized basis set for organic systems B3LYP-6-311 + + G(d,p) was used for all the ground and excited state calculations [24, 25]. The time-dependent density functional theory (TD-DFT) was used with energy minimizations for obtaining the electronic spectra. The energy calculations were set for calculating the 15 states for each combination of PABA and 7DMC and absorption details of crucial transition for each combination were also compared. The molecular electrostatic potential (MEP) surface and counterplots were plotted for each combination to spot the moieties behaving as nucleophilic and electrophilic sites. The Koopman's set of identities mentioned below were used for calculating the global reactivity describing parameters band gap (ΔE), ionization potential (IP), electron affinity (EA), chemical potential (CP), electronegativity (χ), chemical hardness (η), softness (S), electrophilicity index (ω), electropositive index (ω^+), and electronegative index (ω^-) [26, 27]:

$$\Delta E = E_{LUMO} - E_{HOMO} \qquad \dots\dots\dots\dots\dots\dots (1)$$

$$IP = -E_{HOMO} \qquad \dots\dots\dots\dots\dots\dots (2)$$

$$EA = -E_{LUMO} \qquad \dots\dots\dots\dots\dots\dots (3)$$

$$CP = \frac{E_{HOMO} + E_{LUMO}}{2} \qquad \dots\dots\dots\dots\dots\dots (4)$$

$$\chi = \frac{(IP + EA)}{2} \qquad \dots\dots\dots\dots\dots\dots (5)$$

$$\eta = \frac{E_{LUMO} - E_{HOMO}}{2} \qquad \dots\dots\dots\dots\dots\dots (6)$$

$$S = \frac{1}{\eta} \qquad \dots\dots\dots\dots\dots\dots (7)$$

$$\omega = \frac{\mu^2}{2\eta} \qquad \dots\dots\dots\dots\dots\dots (8)$$

$$\omega^{+} = \frac{(IP + 3EA)^2}{16(IP - EA)} \qquad \dots\dots\dots\dots\dots\dots (9)$$

$$\omega^{-} = \frac{(3IP + EA)^2}{16(IP - EA)} \qquad \dots\dots\dots\dots\dots\dots (10)$$

The multiwfn software (http://sobereva.com/multiwfn/) was used to calculate the inter-fragment charge transfer analysis. The IFCT analysis was done to measure the exact amount of charge that has been transferred from the donor and acceptor parts of the designed complex. The transition density matrix (TDM) analysis was performed and the TDM plots were plotted to examine the density of the charge transferred during the excitation. The TDM corresponding to the crucial transition of each of the structures were plotted and interpreted. The electron localization functional surface and molecular isosurfaces were also obtained by the .fchk files of all the considered complexes using multiwfn software.

The Fourier transform-infrared (FT-IR) spectra were plotted by obtaining the vibration data via polar calculations with the same set of functions. The vibrational modes were studied for getting an idea about the responses of the functional groups to the infrared radiation.

The NLO responses of the designed complex were studied using the polarizability parameters like isotropic polarizability (α_{total}), anisotropic polarizability ($\Delta\alpha$), and first-order hyperpolarizability (β_{total}).

$$\alpha_{total} = \frac{1}{2}\left(\alpha_{xx} + \alpha_{yy} + \alpha_{zz}\right) \qquad \ldots\ldots\ldots\ldots\ldots (11)$$

$$\Delta\alpha = \frac{1}{\sqrt{2}}\left[\left(\alpha_{xx} - \alpha_{yy}\right)^2 + \left(\alpha_{yy} - \alpha_{zz}\right)^2 + \left(\alpha_{zz} - \alpha_{xx}\right)^2 + 6\alpha_{xz}^2 + 6\alpha_{xy}^2 + 6\alpha_{yz}^2\right]^{\frac{1}{2}} \ldots\ldots (12)$$

$$\beta_{total} = \left[\left(\beta_{xxx} + \beta_{xyy} + \beta_{xzz}\right)^2 + \left(\beta_{yyy} + \beta_{yzz} + \beta_{yxx}\right)^2 + \left(\beta_{zzz} + \beta_{zxx} + \beta_{zyy}\right)^2\right]^{\frac{1}{2}} \ldots(13)$$

$$\gamma_{total} = \frac{1}{5}\left[\gamma_{xxxx} + \gamma_{yyyy} + \gamma_{zzzz} + 2\gamma_{xxyy} + 2\gamma_{yyzz} + 2\gamma_{xxzz}\right] \ldots\ldots\ldots\ldots (14)$$

where α_{xx}, α_{yy}, and, α_{zz} are the tensor components of polarizability, β_{xxx}, β_{yyy}, and β_{zzz} are the tensor components of first-order hyperpolarizability

3. Results and discussion

3.1 Structural Properties and charge distribution

The optimized geometries of PABA and 7DMC were used for designing the introduced complex (1), (2), and (3) (Fig. 1). The complex (1) was designed by pasting the PABA at a minimal possible distance of 1 Å of 7DMC and the complex was stabilized at the intermolecular distance of approximately 3 Å. The major interactions were seen to form between 12H of PABA and 39H of 7DMC with a distance of 3.6 Å. The major bond lengths related to the functional groups and the reactive sites of all the studied complexes were mentioned in SD 1. The bond lengths corresponding to all the amino groups were of about 1.46 Å and the bond lengths corresponding to the oxygen atoms, carboxyl groups and carboxylic acids have lower bond lengths. The higher bonds length can easily be dissociated when the parent molecule interacts with high intensity field [28]. So, it can be interpreted as the nitrogen atoms with higher bond lengths leads to the generation of the charge cloud. The dipole moment was also analyzed for the introduced complexes. The dipole moment is the quantitative as well as qualitative virtue that tells us about the variation of the charge within the compounds. The higher the dipole moment, the higher will be the chemical reactivity of the compounds [29]. The dipole moment of all the probe and complexed structures were in sequence 7DMC > (1) > PABA > (3) > (2). To this context, the charge distribution among (1), (2), and (3) was also studied and is mentioned in SD 2. The nitrogen atoms involved in all three compounds are observed to contribute positively and the oxygen atoms contribute negatively. Thus, the structural analysis reveals the possibility of the intramolecular as well as intermolecular interactions among (1), (2), and (3).

3.2 Determination of the reactive sites: Nucleophilic and electrophilic moieties

The prediction of the reactive sites in the designed structures was done using molecular electrostatic potential (MEP) surface (Fig. 2) and counterplots (Fig. 3). In (1), the nitrogen atoms were seen to impart positively to the total charge interactions and hence they were surrounded by blue colored surface [30]. The positive nature of the nitrogen atoms may be due to the large electropositive nature of nitrogen in the electrochemical series. Similarly, the oxygen atoms were seen to be surrounded by the red surface revealing the electronegative or charge-deficient nature of these areas. Apart from nitrogen and oxygen atoms, the C-H bonds associated with the benzene rings of 7DMC were seen to participate in charge donation. The light blue colored surface around the C-H bonds reveals the donating nature of C-H bonds and thus, from the MEP surface of (1), it can be stated that the 7DMC majorly acts as a charge donor and PABA acts as a charge acceptor in the adsorbed complex of PABA and 7DMC. The counterplots for (1) indicate the highly accumulated field lines nearby the carboxyl group of PABA and the ketone group of 7DMC. The lightly dense field lines surrounding the rest of the structures show the donation of the charge from nitrogen atoms and C-H bonds of 7DMC [31]. The MEP surface of (2) indicates the electron-excessive nature of the amino group of the PABA molecule and the electron-deficient nature of the ketone group attached to the 7DMC molecule. A similar kind of nature of the reactive locations was observed for (3) in Figure (c) where the PABA and 7DMC were connected with biphenyl. In both complexes (2) and (3), the amino group of PABA acts as a strong electron donor and oxygen atoms act as strong electron-withdrawing groups. Even in the counterplots of (2) and (3), the red-colored field lines indicate the accumulation of the charge cloud was observed over the oxygen atoms and less dense field lines were observed over the rest of the geometry. This behavior was very different and opposite from what we have observed in the adsorbed complex (1) where 7DMC majorly imparts in charge donation and PABA in electron-withdrawing. In (2) and (3), the 7DMC is actively involved as a strong charge-withdrawing agent and PABA acts as electron donating. The reason might be the availability of benzene rings (in connecting π- bridges benzene and biphenyl) that increase the hydrophilic nature of the subject structure due to the excess availability of resonating π double bonds. As a result, the nucleophilic nature of the C-H bonds observed in (1) was terminated in (2) and (3). Thus, the charge transfer was predicted from 7DMC towards PABA in (1), and opposite in bridged complexes (2) and (3).

3.3 Global reactivity descriptors and location of the molecular orbitals

The global reactivity descriptors are a set of parameters that qualitatively reveal the chemical reactivity of the molecules and predict the occurrence of intramolecular interactions within the molecule (SD 3) [32]. The ΔE is the energy gap between the highest occupied and lowest unoccupied molecular orbitals (HOMO-LUMO) and it reveals the gap that the excited electrons have to cover to jump up to the higher energy levels. The lower the gap, the higher the possibility of charge excitation [33]. The band gap of PABA and 7DMC were observed to be 4.775 and 3.691 eV. After the association of PABA and 7DMC, a

drastic reduction in the band gap was observed. The band gap of (1), (2), and (3) was reduced to 3.646, 2.647, and 2.461 eV respectively. The IP and EA for (2) and (3) were also high (2) and (3). IP and EA are the ability of the nucleophile to donate the charge cloud and of the electrophile to withdraw the charge cloud respectively. the higher values of IP and EA for (2) and (3) showed their enhanced chemical reactivity. The CP and χ were also seen to be enhanced. η seen to be decreased for PABA and 7DMC complex. The S value, on the other hand, was increased. The chemical softness was increased which can be interpreted as the increased flexibility of the complexes for undergoing chemical reactions [34]. An extremely drastic increment was observed in the value of ω. ω is the activity of the compounds that are used to express the chemical reactivity of the compounds. The more the value of ω, the more the chemical reactivity of the molecule. Complex (3) has the highest value of ω among the other complexes. A similar kind of increase was noticed in the positive electrophilicity as well as negative electrophilicity. The distribution of the HOMO-LUMO surfaces over the geometries was plotted to predict the charge interactions (Fig. 4). In (1), the orbital surfaces were transferred from PABA to 7DMC. In both (2), and (3), the molecular surfaces were seen to get dislocated from the 7DMC in HOMO to the PABA in LUMO covering the π-bridges. Thus, the global reactivity parameters and molecular orbital surfaces show the high chemical reactivity of the complexes (1), (2), and (3), and the comparison shows that (3) has the best responses for the chemical reactivity.

3.4 Inter-fragment charge transfer analysis

The inter-fragment charge transfer analysis for (1), (2), and (3) was accounted to quantitatively calculate the exact magnitude of the charge transfer from the electron-donor towards the electron-acceptor moiety. The IFCT analysis was carried out in two different ways. Table 1 accounts for the IFCT data when two fragments (fragment 1 of 7DMC and fragment 2 of PABA) were considered in (1), (2), and (3) excluding the bridges (benzene and biphenyl) in (2) and (3) respectively. The IFCT from fragment 1 to fragment 2 was increased as (1) < (2) < (3) and from fragment 2 to fragment 1 decreased as (1) > (2) > (3). The higher amount of charge was seen to be transferred from fragment 2 to fragment 1 which supports the transferring of the charge from PABA to 7DMC. This supported the charge transport path interpreted by the MEP surface and HOMO-LUMO surfaces. The net charge transported from donor to acceptor was higher in (3) (0.03220 e) as compared to (1) (0.0035 e) and (2) (0.01089 e). Observations show that the local excitation percentage was higher for all the complexes as compared to the charge transfer. However, the local excitation was found to be higher for (1). Table 2 accounts for the IFCT results obtained by considering the involvement of the bridges in the charge interactions. After the involvement of the bridges in the IFCT, there seems a rise in the transferred amount of holes and electrons. The bridges were seen to be involved in the intramolecular interactions not so significantly but precisely. However, the charge interaction between fragment 1 (7DMC) and fragment 2 (PABA) was found to be more significant and the net transferred charge between the probe molecular fragments was highest in both the complexes (2) (0.07282 e) and (3) (0.28504 e). Similar to previously performed interpretation without the involvement of the bridges, the local excitation percentage of the charge was found to be higher in later cases (after the

involvement of bridges). The local excitation percentage in **(2)** and **(3)** was 85.903 and 61.795% respectively.

Table 1
Results from the Inter fragment charge transfer (excluding the bridge in **(2)** and **(3)**) of **(1)** adsorbed PABA + 7DMC complex, **(2)** PABA-benzene-7DMC complex, and **(3)** PABA-biphenyl-7DMC complex [IFER-Intra-fragment electron redistribution, IFCT (electrons)- magnitude of the transferred charge, IFCT (%)- percentage of the transferred charge, CT(I)-Intrinsic charge transfer percentage, LE(I)-intrinsic local excitation percentage, CT(A)-apparent charge transfer percentage, LE(A)-apparent local excitation percentage].

Properties		(1)	(2)	(3)
Fragment 1 (7DMC)	Hole (%)	99.24	96.15	95.08
	Electron (%)	99.62	88.84	63.36
Fragment 2 (PABA)	Hole (%)	0.76	0.32	0.25
	Electron (%)	0.38	1.43	3.56
IFER	IFER (1)	0.98860	0.85420	0.60243
	IFER (2)	0.00003	0.00005	0.00009
IFCT (electrons)	1→2	0.00381	0.01376	0.03381
	2→1	0.00756	0.00286	0.00161
	Net charge	0.00375	0.01089	0.03220
IFCT (%)	CT (I)	1.137	1.662	3.542
	LE (I)	98.863	85.424	60.252
	CT (A)	0.375	1.089	3.220
	LE (A)	99.625	98.911	96.780

Table 2
Results from the Inter fragment charge transfer (including the bridge in (2) and (3)) of (1) adsorbed PABA + 7DMC complex, (2) PABA-benzene-7DMC complex, and (3) PABA-biphenyl-7DMC complex [IFER-Intra-fragment electron redistribution, IFCT (electrons)- magnitude of the transferred charge, IFCT (%)-percentage of the transferred charge, CT(I)-Intrinsic charge transfer percentage, LE(I)-intrinsic local excitation percentage, CT(A)-apparent charge transfer percentage, LE(A)-apparent local excitation percentage].

Properties		(2)	(3)
Fragment 1 (7DMC)	Hole (%)	96.15	95.08
	Electron (%)	88.84	63.36
Fragment 2 (PABA)	Hole (%)	26.08	0.25
	Electron (%)	0.21	3.56
Fragment 3 (Bridge)	Hole (%)	3.85	4.66
	Electron (%)	11.13	33.09
IFER	IFER (1)	0.85420	0.60243
	IFER (2)	0.00056	0.00009
	IFER (3)	0.00428	0.01543
IFCT (electrons)	$1 \rightarrow 2$	0.00206	0.03381
	$2 \rightarrow 1$	0.23172	0.00161
	Net charge	-0.22966	0.03220
	$1 \rightarrow 3$	0.10698	0.31459
	$3 \rightarrow 1$	0.03416	0.02955
	Net charge	0.07282	0.28504
	$2 \rightarrow 3$	0.02902	0.00084
	$3 \rightarrow 2$	0.00008	0.0017
	Net charge	0.02894	-0.00082
IFCT (%)	CT (I)	40.402	38.205
	LE (I)	85.903	61.795

3.5 Electron localization function (ELF) and molecular isosurface analysis

The ELF surface provides insights into electron localization in molecular geometry. The red patches obtained in the ELF surfaces of (1), (2), and (3) denote the availability of the electrons (Fig. 5). In the ELF surface of (1), most of the red-colored spots were obtained over the 7DMC molecule and such spots were absent from the PABA geometry. Moreover, the green bulged-out figure shown above the ELF surfaces is the mapping of the ELF surface that helps in directly locating the available electrons. The bulged-out area is where the electrons exist and it was observed that the fully grown peaks were observed over the 7DMC molecule whereas in the case of PABA, the peaks have a cavity at the top. A similar kind of behavior was obtained in (2) and (3) as well. the higher peaks in the mapping and the red spots were located all over the 7DMC molecule and the availability of the electrons was also supported by the settlement of the molecular isosurface. Therefore, the ELF and isosurface settlement suggests that the charge is being transported from the 7DMC towards the PABA in the complexes.

3.6 Transition state optimizations

The electronic transitions (for nine prominent transitions) were studied by computing the absorption spectra of all the title complexes using energy minimizations with the same set of basis functionals. The details of the transitions have been listed in SD 4. The absorption spectra for adsorbed PABA + 7DMC complex, PABA-benzene-7DMC complex, and PABA-biphenyl-7DMC complex with crucial transition details have been labeled and illustrated in Fig. 6. The absorption spectra with two peaks were observed between 200–300 nm and 300–450 nm for (1), the first band being higher in intensity than the second band. The crucial transition for the first band ($S_0 \rightarrow S_6$) was observed at 278 nm with an oscillator strength of 0.1913 and the crucial transition of the second band ($S_0 \rightarrow S_2$) was observed at 353 nm with an oscillator strength of 0.3133. As the aromatic bridges were introduced in the combinations, the absorption intensity of the spectra of (2) and (3) were observed to be increased. Same as (1), the absorption spectra of (2) with two bands of nearly equal intensity were obtained between 250–300 and 300–450 nm. The crucial transitions in both the bands were observed at 352 nm and 274 nm with increased values of oscillator strength of 0.7484 and 0.1004 respectively. In (3), one prominent absorption band was observed between 250–450 nm with one shoulder band and one peak at 304 and 372 nm respectively. The oscillator strengths of these crucial transitions were obtained as 0.5040 and 1.0845. There has been a significant rise in the oscillator strength of the aromatic bridged complexes of PABA and 7DMC. This shows the ease in the occurrence of electronic transitions in the bridge-connected complexes. Moreover, the shift in the peak's wavelength was also noticed manifesting the bathochromic shift in the peak wavelength of (2) and (3). The peak wavelengths of (2) and (3) were readily shifted towards the ultraviolet region showing the π–π* nature of the undergone transitions in the complexes [35]. Therefore, several incredible observations in the absorption spectra of (1), (2), and (3) like increased oscillator strength, shift in the wavelength of the peaks towards the higher ranges, increased intensity of the spectra, and increased excitation energy of the transitions validates the high absorptive nature of the proposed complexes and proves that the complex has potential to carry the electronic transitions and become chemically reactive.

3.7 Transition density matrix (TDM) analysis

The TDM plots were obtained for the $S_0 \rightarrow S_2$ transition of (1), and $S_0 \rightarrow S_1$ transition of (2) and (3) (Fig. 7). The TDM plots are used to locate the moieties dominating the holes, electrons, and excited state of the electrons. These plots generally explain the exciton coherence with the help of diagonal (locally excited) character and off-diagonal (charge transfer) character. The hydrogen atoms of the molecules generally don't impart in the excitation of the charge and thus, they are not involved in the TDM calculations. In (1), the 7DMC acts as the donor and PABA acts as the acceptor and hence the exciton coherence in (1) was found to be majorly distributed towards the upper diagonal area with high charge value and the darker area showing the availability of the holes was found to be near the lower axis area. The nature of the TDM plots in (2) and (3) differs from that of (1) due to the involvement of the π-linker or bridges. The π-bridges act as a pathway for efficient charge transfer characteristics. The presence of different aromatic rings as π-bridges enhances the donor capability of a molecule. The exciton coherence in (2) and (3) was obtained near the diagonal areas indicating the electron cloud near the nitrogen atoms and the dark patches indicating the holes that seem the larger portion of the transition map was located at the diagonal location. In (1) and (2), the electron location behavior is similar suggesting that π-linkers modification is an efficient approach for enhancing the charge-donating capability of a molecule.

3.8 Vibrational modes analysis

The vibrational assignments corresponding to each complex were accounted by the title complexes to check the availability as well as the involvement of the functional groups and the interconnecting aromatic bridges in increasing the chemical polarizability of the introduced complexes. The well-labeled FT-IR spectra for (1), (2), and (3), were illustrated in Fig. 8. The prominent peaks for the FT-IR were observed in the range $250-2000$ cm^{-1}, so the spectra were illustrated in the aforementioned range for all the considered complexes. Major modes in FT-IR spectra of (1) with higher peaks were observed for symmetric stretching (ν) of C = O bonds (1754 cm^{-1}) and C = C bonds (1655 cm^{-1}), torsional bending (δ) of C = N (1446 cm^{-1}), C-H (1181 cm^{-1}), and in-plane twisting (τ) of N-H (645 and 1092 cm^{-1}) bonds. In the C = C, C = N, and C-H vibrational modes, the bonds associated with the surface contact between PABA and 7DMC were observed to significantly vibrate as compared to the bonds of the rest of the geometries of PABA and 7DMC. This not only ensures the suitable adsorption site for both PABA and 7DMC but also reports the formation of strong H-bond interactions that occurred at the absorption site between both molecules. After the introduction of benzene as a π-bridge between PABA and 7DMC in (2), the number of peaks in FT-IR spectra was observed to increase. Two peaks for τ_{NH} were obtained at 458 and 1083 cm^{-1}. The bending assignments of C-H bonds were observed to give multiple peaks in between $1000-1250$ cm^{-1} with the most prominent peaks at 1193 and 1276 cm^{-1}. The peak of δ_{CN} was observed at 1552 cm^{-1}. The $\nu_{C=C}$ mode in (2) was observed at the same frequency as in (1) i.e., at 1655 cm^{-1} but the $\nu_{C=C}$ mode in (2) was slightly shifted at 1775 cm^{-1}. Similar to (2), the number of prominent peaks in (3) for FT-IR was also increased. The peaks of τ_{NH} were obtained at 394, 1030, and 1087 cm^{-1}. The δ_{CH} modes were observed at 1204 and 1309 cm^{-1}. The $\nu_{C=C}$ mode was the one with the highest peak at 1707 cm^{-1}. The $\nu_{C=O}$ mode gave two strong peaks at higher frequencies at 1664 and 1750 cm^{-1}. The increment in

the number of peaks was observed as a result of the involvement of the benzene (in **(2)**) and biphenyl (in **(3)**) rings as the π-bridges. The reason could be the resonating nature of the aromatic bridges that results in the redistribution of the energy among different perturbed levels despite of the single unperturbed level [36]. This gave rise to multiple peaks of FT-IR for a single kind of vibrational assignment (as per the Frank-Condon envelope spectra theory) [37]. Additionally, it can be stated that the involvement of the π-bridges makes the resultant complex (**(2)** and **(3)**) respond to the IR radiation more vigorously as compared to the adsorbed complex **(1)**. Therefore, the increased number of vibrational assignments and increased frequencies of the modes tell us that the proposed complexes were chemically reactive and highly polarizable.

3.9 Linear and nonlinear behavior of materials

A comparison of all the NLO parameters for the proposed complex was illustrated in Fig. 9 (SD 5). The coefficient of lower order terms like α_{total} and $\Delta\alpha$ is used to check the optical linearity of the compounds. The α_{total} accounts for the isotropic polarizability of the compounds. Symmetric/centrosymmetric compounds were believed to possess a high value of α_{total}.[38]. Mostly the compounds with uniform properties throughout have a higher value of α_{total}. The α_{total} of all the compounds was observed to be in the increasing order of PABA < 7DMC < **(1)** < **(2)** < **(3)**. This reveals the isotropic nature of the π-bridged compounds. The anisotropic nature, on the other hand, accounts for the $\Delta\alpha$ value of the compounds. The $\Delta\alpha$ value of the complexes were in sequence **(1)** < **(2)** < **(3)**. Thus, the polarizability parameters suggest the enhanced extent of polarization of the complexes with the increasing number of benzene rings in the bridge [39]. The nonlinear behavior of the compounds is suggested by the coefficients of higher-order terms of the expansion of energy in high-intensity fields i.e., β_{total} and γ_{total} [40]. The β_{total} is the parameter that helps in justifying the NLO responses of the target compound. The higher value of β_{total} shows that the considered compound provides a tough medium to the high-intensity field lines and the compound strongly interacts with the light. In the present case, the value of β_{total} was found to be highest for **(1)** followed by **(3)**, and then **(2)**. The γ_{total} reports the second-order NLO responses of the compounds. Mostly, it is used to computationally predict the occurrence of the saturable absorption (or reverse saturable absorption) in the compounds [41]. The positive value of γ_{total} confirms saturable absorption and the negative value of γ_{total} shows the occurrence of reverse saturable absorption [42]. The value of γ_{total} increases as the number of benzene rings increases in the π-bridge as **(1)** < **(2)** < **(3)**. Thus, the occurrence of reverse saturable absorption can be predicted for the proposed complexes. Moreover, the aforementioned statement can say to be reliable and the present study can be used as a pre-assumed theory as both PABA and 7DMC were experimentally proven to possess reverse saturable absorption and there might be a strong possibility to get the same, and enhanced results with the combination of these compounds. Additionally, it was observed that as compared to the probe PABA and 7DMC, the combination of both these compounds has better and more promising NLO activity. Therefore, the NLO parameters suggest that the combinations of PABA and 7DMC work as more promising NLO materials.

4. Conclusion

The present study gives a theoretical understanding of the combination of PABA and 7DMC. The higher bond lengths for amino groups and the lower bond lengths of carboxyl groups suggest the easy dissociation tendency of the amino group. the dissociation of amino groups shows the generation of the charge cloud from the amino group. The MEP surface and the counterplots suggest the nucleophilic nature of amino groups and the electrophilic nature of carboxyl groups in the complex. The absorption peak was seen to get shifted towards the longer wavelength with higher intensity showing the increased chemical reactivity of the complex. The vibrational peaks corresponding to each mode are also seen to increase in the numbers which shows the increased response of the combinations towards the infrared radiation. Lastly, the β_{total} and γ_{total} values were seen to increase for the combinations. The increment in the values of hyperpolarizability parameters validates strong candidature of the combination of PABA and 7DMC to be used for NLO applications. Thus, the reported work makes a strong foundation for pursuing the experimental work with the combination of two compounds PABA and 7DMC.

Declarations

Ethical Approval

This material is the author's original work, which has not been previously published elsewhere. All authors have been personally and actively involved in substantial work leading to the paper and will take public responsibility for its content. The paper properly credits the meaningful contributions of all the co-authors.

Competing interests

The authors declare that they have no known competing financial interests or personal relationships that could have appeared to influence the work reported in this paper.

Authors' contributions

Shradha Lakhera: Data curation, Writing-Original draft preparation, Visualization, Investigation, Software, Validation.

Meenakshi Rana: Conceptualization, Methodology, Writing-Reviewing and Editing, Supervision

Kamal Devlal: Conceptualization, Writing- Reviewing and Editing

Funding

Availability of data and materials

All data generated or analyzed during this study, which support the plots within this paper and the other findings of this study, are included in this article and its supplementary information. Source data are provided in this paper.

References

1. M. J. Cho, D. H. Choi, P. A. Sullivan, A. J. P. Akelaitis, L. R. Dalton, Recent progress in second-order nonlinear optical polymers and dendrimers. Prog. Polym. Sci. 33 (11) (2008) 1013-1058. https://doi.org/10.1016/j.progpolymsci.2008.07.007

2. W. M. Sun, D. Wu, Y. Li, Z. R. Li, Theoretical study on superalkali (Li_3) in ammonia: novel alkalides with considerably large first hyperpolarizabilities. Dalt Trans 43 (2014) 486–494. https://doi.org/10.1039/c3dt51559a

3. S. B. Kolavekar, N. Ayachit, G. Jagannath, K. NagaKrishnakanth, S. R. Rao, Optical, structural and Near-IR NLO properties of gold nanoparticles doped sodium zinc borate glasses. Opt Mater. 83 (2018) 34–42. https://doi.org/10.1016/j.optmat.2018.05.083

4. I. Jeon, A. Shawky, H. S. Lin, S. Seo, H. Okada, J. W. Lee, A. Pal, S. Tan, A. Anisimov, E. I. Kauppinen, Controlled redox of lithium-ion endohedral fullerene for efficient and stable metal electrode-free perovskite solar cells. J Am Chem Soc. 141 (2019) 16553–16558. https://doi.org/10.1021/jacs.9b06418

5. P. Kaur, K. SinghSecond-order nonlinear polarizability of "Push-Pull" chromophores. A decade of progress in donor-π-acceptor materials. JACS. (2022) e202200024. https://doi.org/10.1002/tcr.202200024

6. S. Prabu, N. Palanisami, Aggregation induced emission (AIE)-active ferrocene conjugated linear π–extended multi donor−π−acceptor (D-D'-π-A) chromophores: Synthesis, structural, theoretical, linear and nonlinear optical studies. Dyes Pigm. 201 (2022) 110193. https://doi.org/10.1016/j.dyepig.2022.110193

7. S. Marder, B. Kippelen, Y. A. Jen, et al. Design and synthesis of chromophores and polymers for electro-optic and photorefractive applications. Nature. 388 (1997) 845–851. https://doi.org/10.1038/42190

8. J. Liu, C. Ouyang, F. Huo, W. He, A. Cao, Progress in the enhancement of electro-optic coefficients and orientation stability for organic second-order nonlinear optical materials. Dyes Pigm. 181 (2020) 108509. https://doi.org/10.1016/j.dyepig.2020.108509

9. A. V. Cunha, R. W. A. Havenith, J. V. Gog, D. F. Vleeschouwer, P. F. DE, W. Herrebout, The Halogen Bond in Weakly Bonded Complexes and the Consequences for Aromaticity and Spin-Orbit Coupling. *Molecules*. 28 (2) (2023) 28(2). https://doi.org/10.3390/molecules28020772

10. S. Ma, W. Zhao, J. Zhou, J. Wang, S. Chu, Z. Liu, G. Xiang A new type of noncovalent surface−p stacking interaction occurring on peroxide-modified titania nanosheets driven by vertical p-state

polarization. Chem. Sci. 12 (2021) 4411–4417. https://doi.org/10.1039/d0sc06601j

11. A. Aathif Basha, F. Liakath Ali Khan, S. Muthu, Predhanekar Mohamed Imran, Attar Kubaib, Dielectric relaxation, dipole moment, electronic characterization and non-covalent interaction behavior of valeramide and halo-phenol in non-polar liquid: A density functional theory-based approach. J. Mol. Liq. 370 (2023) 121027. https://doi.org/10.1016/j.molliq.2022.121027

12. R. Deul, E. U. Franck, The Static Dielectric Constant of the Water-Benzene Mixture System to 400°C and 2800 bar. 95 (8) (1991) 847-853 https://doi.org/10.1002/bbpc.19910950801

13. Supreet, G. Singh, Recent advances on cadmium free quantum dots-liquid crystal nanocomposites. Applied Materials Today. 21 (2020) 100840. https://doi.org/10.1016/j.apmt.2020.100840

14. S. Bhattacharjee, A. Banerjee, K. K. Chattopadhyay, Field-enhanced polarization in polytype ferric oxides: confronting anisotropy in dielectric ellipsoid dispersion. *J. Phys. D: Appl. Phys.* 54 (29) (2021) 295301. https://doi.org/10.1088/1361-6463/abf806

15. M.Dréano, O. Mongin, F. Paul, M. G. Humphrey, Nonlinear optics: from theory to applications, with a focus on the use of two-photon absorption in biology. Aust. J. Chem. 76(3) (2023) 130-149. https://doi.org/10.1071/CH23015

16. C. Fan, C. Li, M. Q. Zhu, Dynamic Super-resolution Fluorescence Imaging Based on Photo-switchable Fluorescent Spiropyran. JACS. 128 (13) (2006) 4303–4309. https://doi.org/10.1002/9781119643098.ch46

17. T. P. Gerasimova, A. R. Sirazieva, S. A. Katsyuba, A. A. Kalinin, L. N. Islamova, G. M. Fazleeva, A. A. Shustikov, A. G. Shmelev, A. B. Dobrynin, O. G. Sinyashin, The role of acceptor and π-bridge for donor-driven halochromism of D-π-A N,N-dialkylaminostyrylhetarenes. Dyes Pigm. 210 (2023) 110949. https://doi.org/10.1016/j.dyepig.2022.110949

18. R. Kumar, S. K. Yadav, R. Seth, et al. Designing of gigantic first-order hyperpolarizability molecules via joining the promising organic fragments: a DFT study. J Mol Model. 29 (2023) 5. https://doi.org/10.1007/s00894-022-05401-7

19. Y. C. Feng, Z. B. Cai, S. Li, L. J. Chen, Q. Ye, Y. P. Tian, Novel V-shaped D-π-A-π-D two-photon absorption compounds with large Stokes shifts: Synthesis, optical properties, selective detection of cysteine, and imaging in living cells. Dyes Pigm. 210 (2023) 111021. https://doi.org/10.1016/j.dyepig.2022.111021

20. S. Lakhera, M. Rana, K. Devlal, S. Sharma, P. Chowdhury, V. Dhuliya, S. Panwar, Sagar L. P. Purohit, A. Dhanusha, T. C. Girisun, Exploring the Nonlinear Optical Limiting Activity of Para-Aminobenzoic Acid by Experimental and Dft Approach. J. Photochem. Photobiol. (2023) 114987. https://doi.org/10.1016/j.jphotochem.2023.114987

21. S. Lakhera, M. Rana, K. Devlal, N. Kanagathara, A. Dhanusha, T. C. Sabari Girisun, Shruti Sharma, Papia Chowdhury, Nonlinear Optical and Optical Limiting Activity of 7-Diethylamino-4-methylcoumarin/dimethyl formamide solution, Journal of Photochemistry & Photobiology, A: Chemistry (2023) (Under review).

22. M. J. Frisch, Gaussian 09, Revision B.01, Gaussian Inc., Wallingford CT (2010)

23. D. Roy, K. Todd, Millam, J. M. Semichem, GaussView, Version 6, Inc., Shawnee Mission, KS (2016).

24. A. D. Becke, Density-functional thermochemistry. III. The role of exact exchange, J. Chem. Phys. 98 (1993) 5648. https://doi.org/10.1063/1.464913

25. A. D. Becke, Density-functional thermochemistry. V. Systematic optimization of exchange-correlation functionals. J. Chem. Phys. 107 (1997) 8554–8560. https://doi.org/10.1063/1.475007

26. S. Lakhera, K. Devlal, A. Ghosh, M. Rana, Modelling the DFT structural and reactivity study of feverfew and evaluation of its potential antiviral activity against COVID-19 using molecular docking and MD simulations. Chem. Pap. 76 (2022) 2759–2776. https://doi.org/10.1007/s11696-022-02067-6

27. S. Lakhera, K. Devlal, M. Rana, I. Celik, Study of nonlinear optical responses of phytochemicals of Clitoria ternatea by quantum mechanical approach and investigation of their anti-Alzheimer activity with in silico approach. Struct Chem (2022). https://doi.org/10.1007/s11224-022-01981-5

28. Q. Cheng, X. Shi, C. Li, Y. Jiang, Z. Shi, J. Zou, X. Wang, X. Wang, Z. Cui, Chromophores with side isolate groups and applications in improving the poling efficiency of second non-linear optical (NLO) materials. Dyes Pigm. 162 (2019) 721-727. https://doi.org/10.1016/j.dyepig.2018.11.001

29. V. Krishnakumar, R. Nagalakshmi, Studies on the first-order hyperpolarizability and terahertz generation in 3-nitroaniline. Phys. B: Condens. Matter. 403 (10) (2008) 1863-1869. https://doi.org/10.1016/j.physb.2007.10.341

30. R. Thirumurugan, B. Babu, K. Anitha, J. Chandrasekaran, Synthesis, growth, characterization and quantum chemical investigations of a promising organic nonlinear optical material: Thiourea-glutaric acid, J. Mol. Struct. 1171 (2018) 915-925. https://doi.org/10.1016/j.molstruc.2017.07.027

31. M. Faizan, M. Mehkoom, Z. Afroz, V. H. N. Rodrigues, S.M. Afzal, S. Ahmad, Experimental and computational investigation of novel dihydrated organic single crystal of 2,4,6-triaminopyrimidine and 3,5-dintrobenzoic acid: Linear and nonlinear optical response with limiting performance. J. Solid State Chem. 300 (2021) 122255. https://doi.org/10.1016/j.jssc.2021.122255

32. M. T. O. Abe, C. L. Nzia, L. S. Sidjui,. et al. Predictive calculation of structural, nonlinear optical, electronic and thermodynamic properties of andirobin molecule from ab initio and DFT methods. SN Appl. Sci. 3 (2021) 768. https://doi.org/10.1007/s42452-021-04749-4

33. S. Lakhera, K. Devlal, M. Rana, Investigation of the electronic and optical activity of halogen-substituted 2-nitrotoulene by density functional theory. Opt Quant Electron. 55 (2023) 292. https://doi.org/10.1007/s11082-023-04569-3

34. S. Lakhera, K. Devlal, A. Ghosh, M. Rana, In Silico Investigation of Phytoconstituents of Medicinal Herb Piper Longum Against SARS-CoV-2 by Molecular Docking and Molecular Dynamics Analysis, Results in Chemistry. (2021) 100199. https://doi.org/10.1016/j.rechem.2021.100199

35. J. S. A. Otaibi, Y. S. Mary, Y. S. Mary, Understanding the mechanism of thioguanine's binding to Ag6 and bimetallic (Ag3–Au3 and Ag3–Cu3) clusters, J. Mol. Struct. 1265 (2022) 133415. https://doi.org/10.1016/j.molstruc.2022.133415

36. A. C. L. Moreira, V. Lenzi, L. S. Marques, Electronic transport through odd-even methylenic spacers connected to an aromatic ring. Comput. Mater. Sci. 197 (2021) 110596. https://doi.org/10.1016/j.commatsci.2021.110596

37. R. Kumar, A. Kumar, V. Deval, A. Gupta, P. Tandon, P. S. Patil, P. Deshmukh, D. Chaturvedi, J. G. Watve, Molecular structure, spectroscopic (FT-IR, FT Raman, UV, NMR and THz) investigation and hyperpolarizability studies of 3-(2-Chloro-6-fluorophenyl)-1-(2-thienyl) prop-2-en-1-one. J. Mol. Struct. 1129 (2017) 292-304. https://doi.org/10.1016/j.molstruc.2016.09.087

38. S. Lakhera, K. Devlal, M. Rana, V. Dhuliya, N. Pandey, Non-Linear Optical Behavior of 2,9-Dimethylquinacridone with Adsorbed Gold and Silver Nanoclusters, Optik. (2023) 170983. https://doi.org/10.1016/j.ijleo.2023.170983

39. S. Lakhera, K. Devlal, M. Rana, V. Dhuliya, Computational study of non-linear optical and electrical properties of 1,3-dinitropyrene. Opt Quant Electron. 55 (2023) 85. https://doi.org/10.1007/s11082-022-04371-7

40. S. Lakhera, M. Rana, K. Devlal, N. Kanagathara, J. Janczak, Photovoltaic Characteristics of Organic Heterocyclic2,9-dimethyl Quinacridone in Different Solvents Using DFT Approach. J. Photochem. Photobiol. (2023) 114664. https://doi.org/10.1016/j.jphotochem.2023.114664

41. M. Nakano, S. Yamadu, K. Yamaguchi, Negative Second Hyperpolarizability of the Nitronyl Nitroxide Radical. CSJ Journals. 71 (4) (1998) 845-850. https://doi.org/10.1246/bcsj.71.845

42. A. Swamynayaka, K. Venkatesha, K. K. Harish, B. N. Revanna, C.Venkatesh, M. Madegowda, T. A. Hegde, Third-order nonlinear response of a novel organic acetohydrazide derivative: Experimental and theoretical approach. Opt. Mater. 139 (2023) 113826. https://doi.org/10.1016/j.optmat.2023.113826
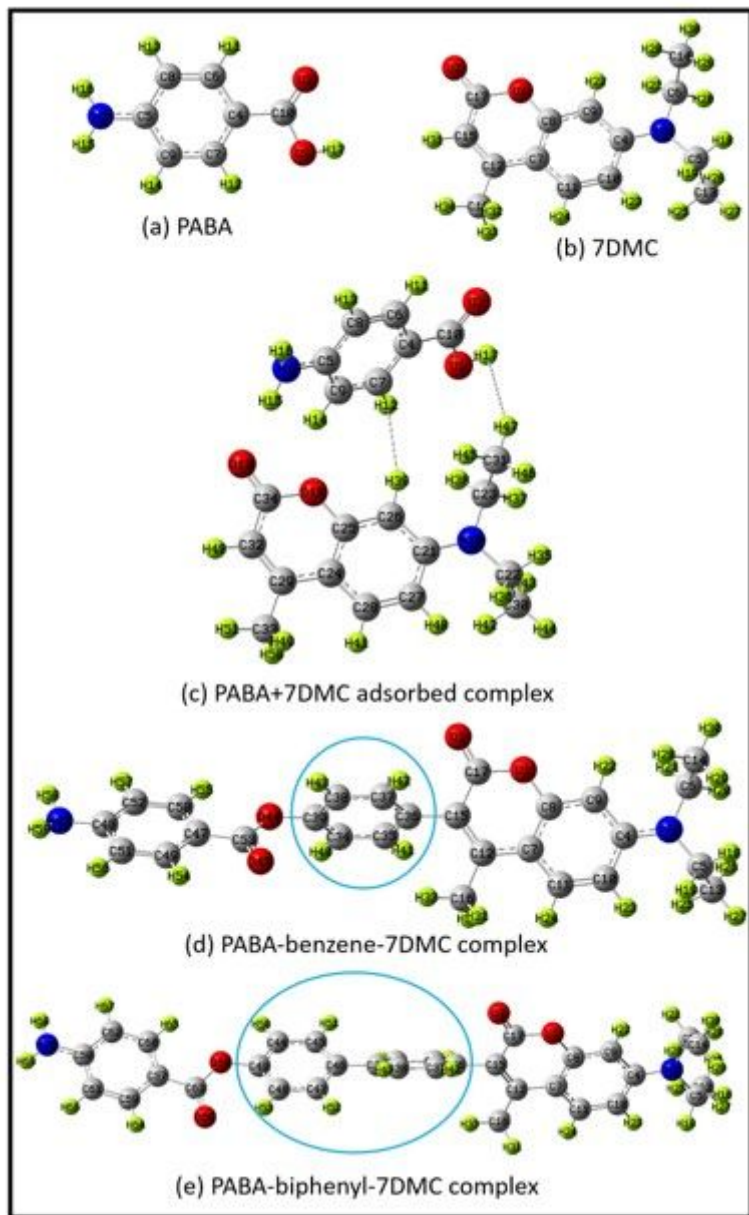
Figures

Figure 1

Optimized geometries of (a) PABA, (b) 7DMC, (c) adsorbed PABA+7DMC complex, (d) PABA-benzene-7DMC complex, and (e) PABA-biphenyl-7DMC complex with B3LYP-6-311++G(d,p).
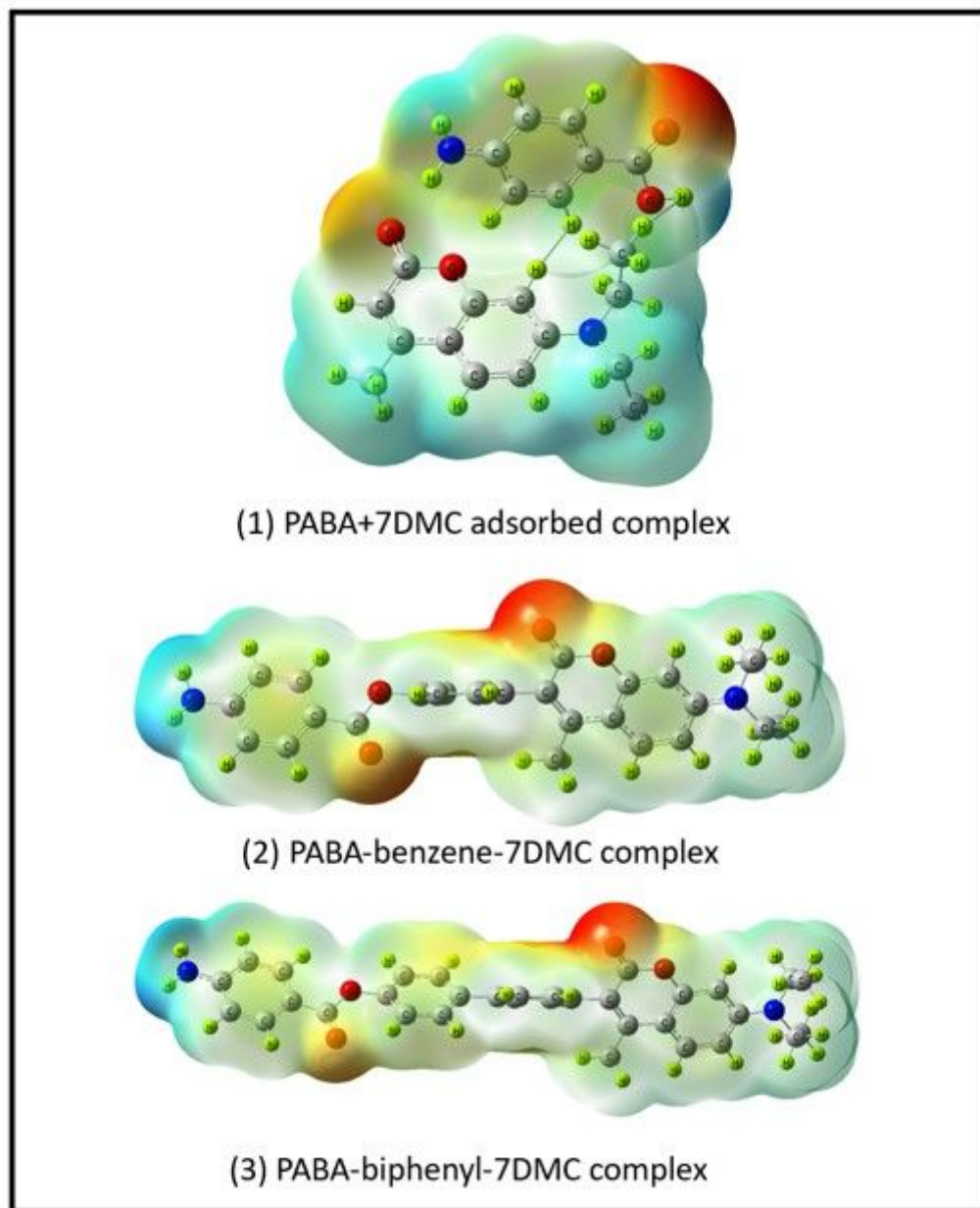
(1) PABA+7DMC adsorbed complex

(2) PABA-benzene-7DMC complex

(3) PABA-biphenyl-7DMC complex

Figure 2

Molecular electrostatic potential surfaces of **(1)** adsorbed PABA+7DMC complex, **(2)** PABA-benzene-7DMC complex, and **(3)** PABA-biphenyl-7DMC complex.
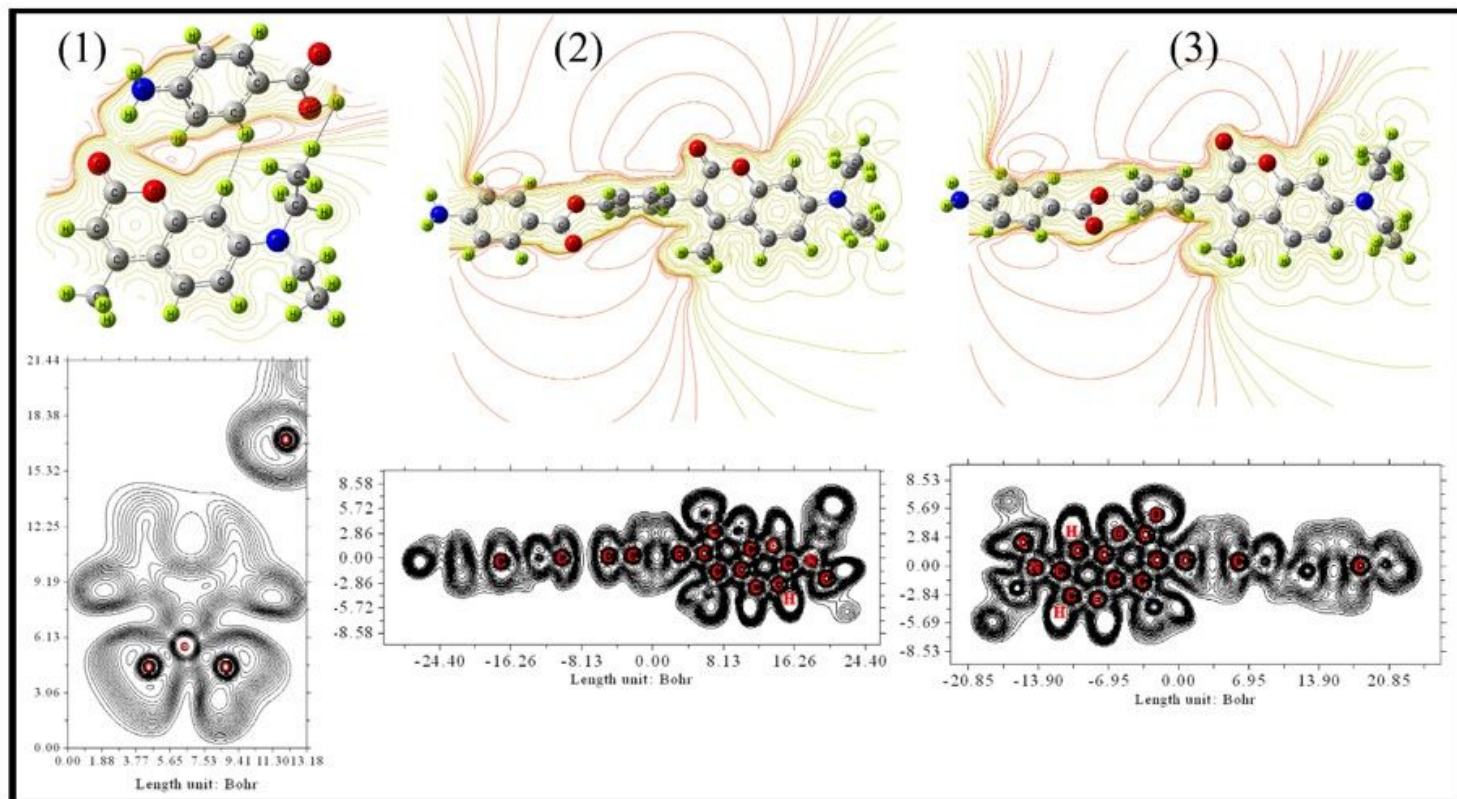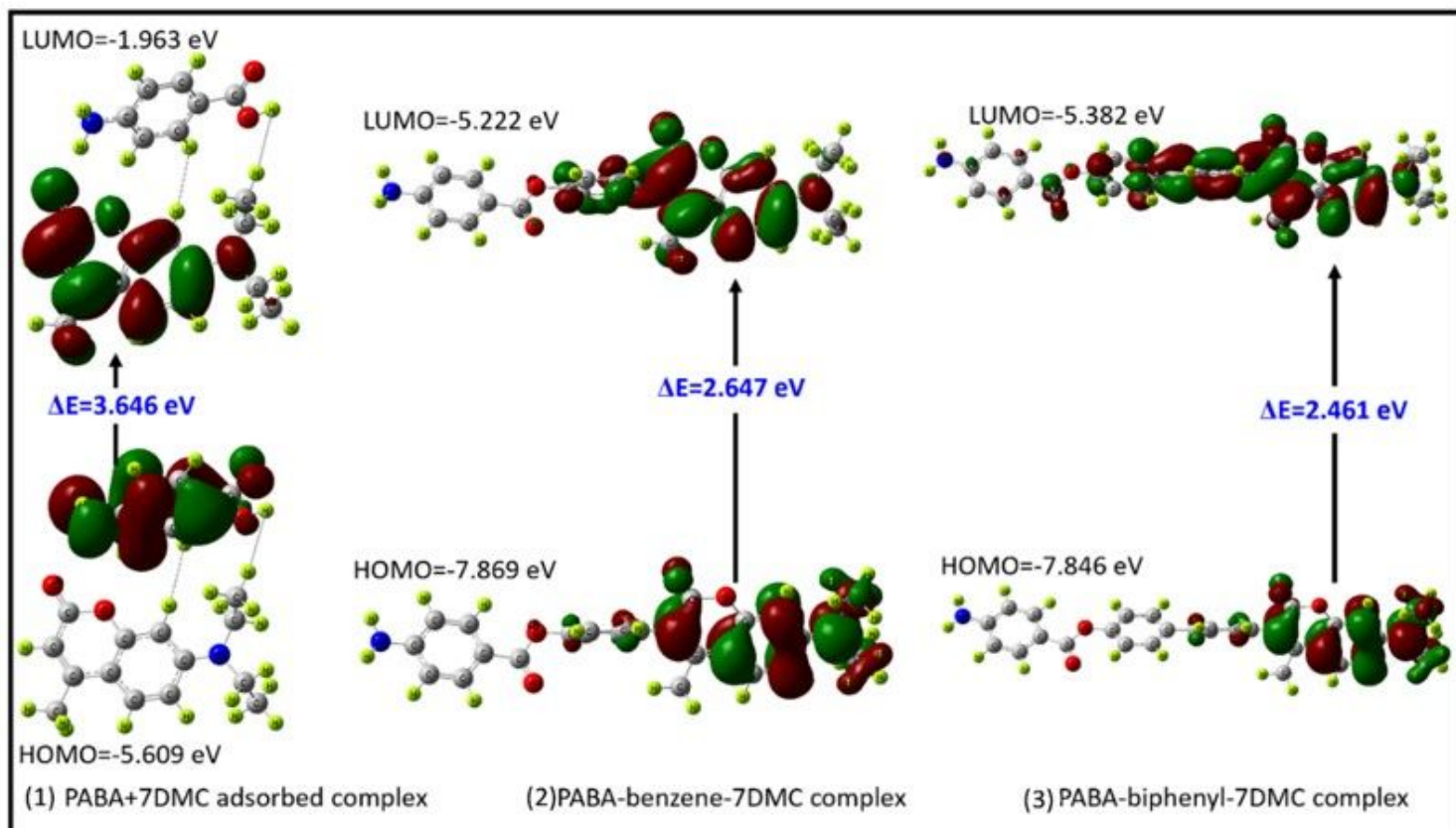
Figure 3

Molecular electrostatic potential surfaces of **(1)** adsorbed PABA+7DMC complex, **(2)** PABA-benzene-7DMC complex, and **(3)** PABA-biphenyl-7DMC complex.

Figure 4

Location of the molecular orbitals of **(1)** adsorbed PABA+7DMC complex, **(2)** PABA-benzene-7DMC complex, and **(3)** PABA-biphenyl-7DMC complex.
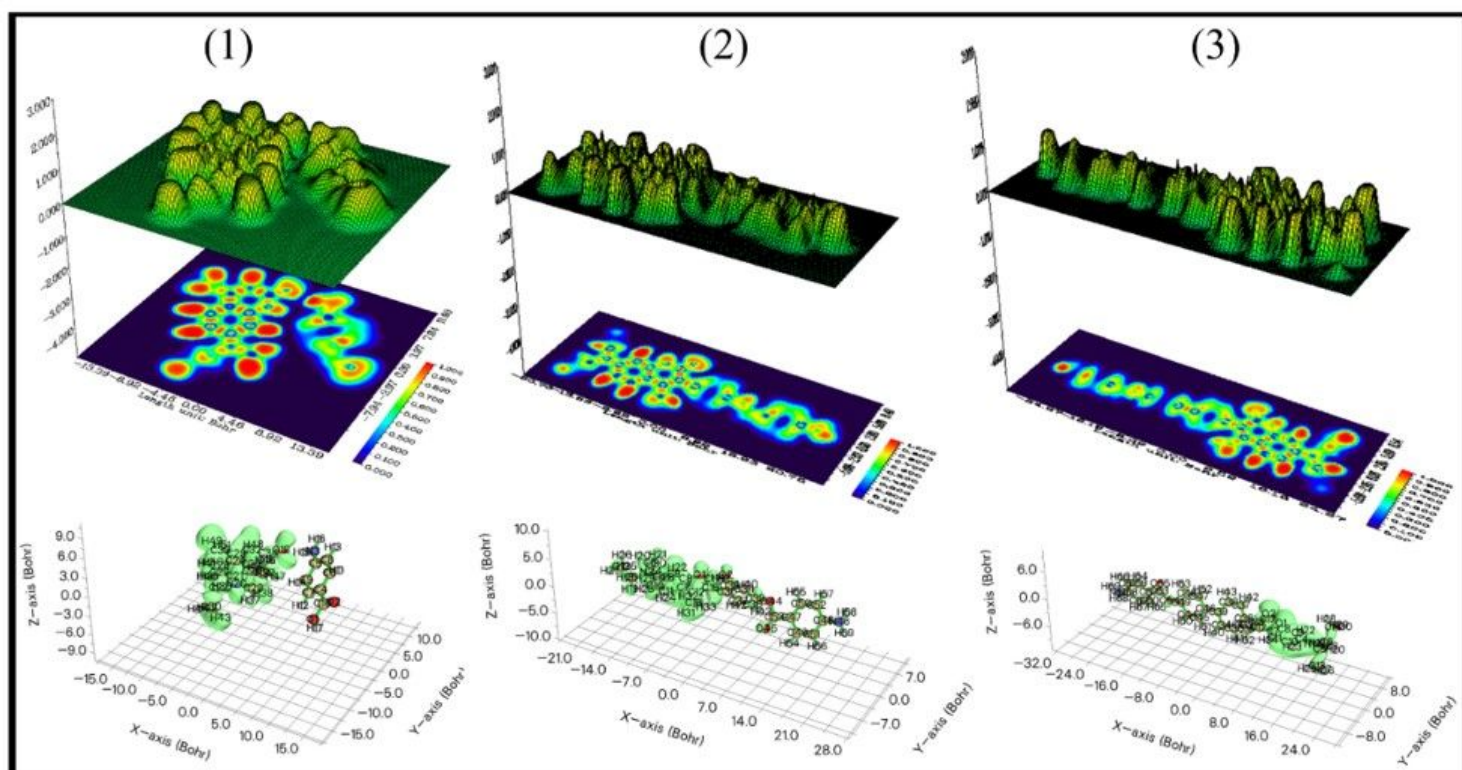
Figure 5

ELF and molecular isosurface of **(1)** adsorbed PABA+7DMC complex, **(2)** PABA-benzene-7DMC complex, and **(3)** PABA-biphenyl-7DMC complex.
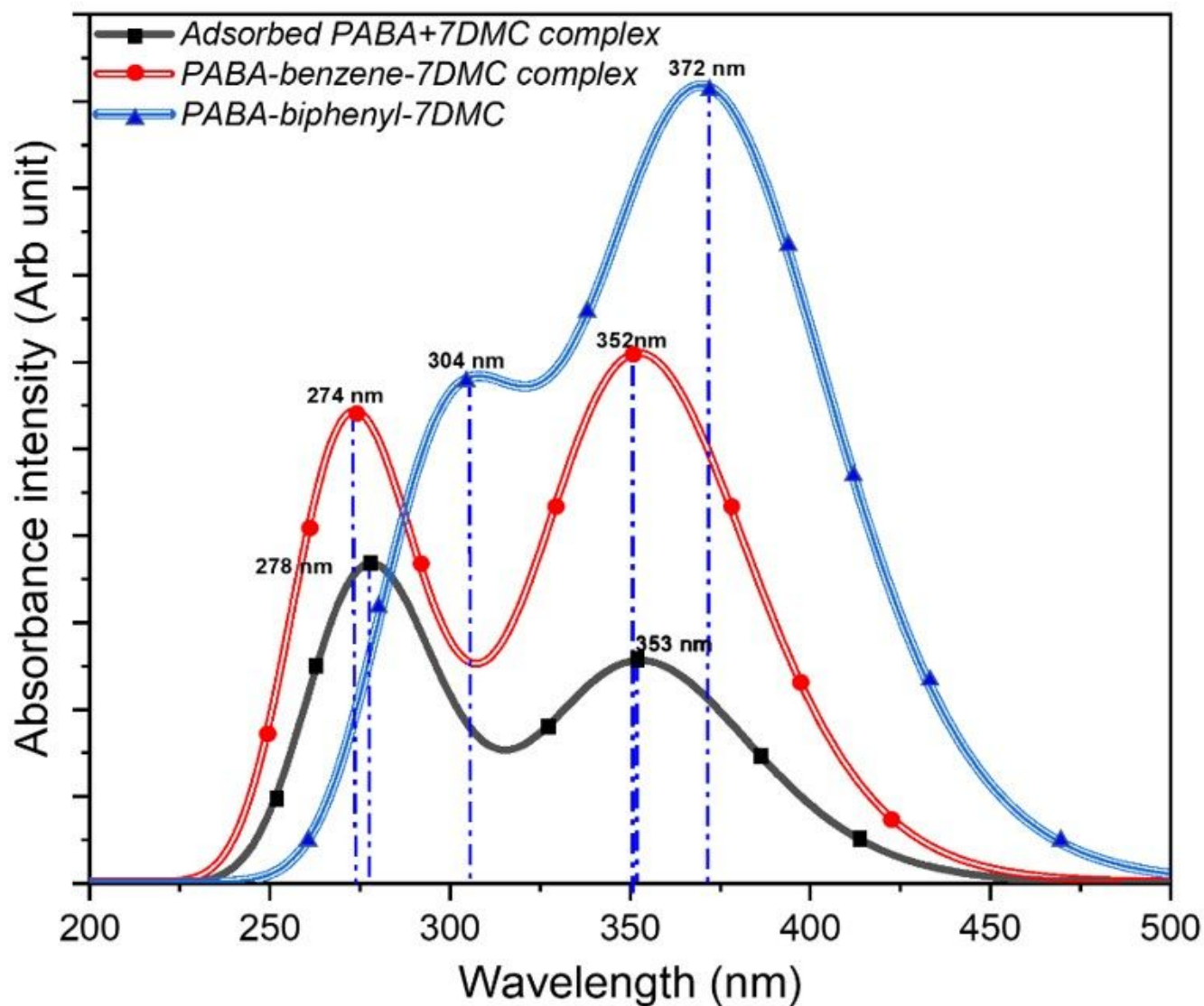
Figure 6

Computed absorption spectra of **(1)** adsorbed PABA+7DMC complex, **(2)** PABA-benzene-7DMC complex, and **(3)** PABA-biphenyl-7DMC complex.
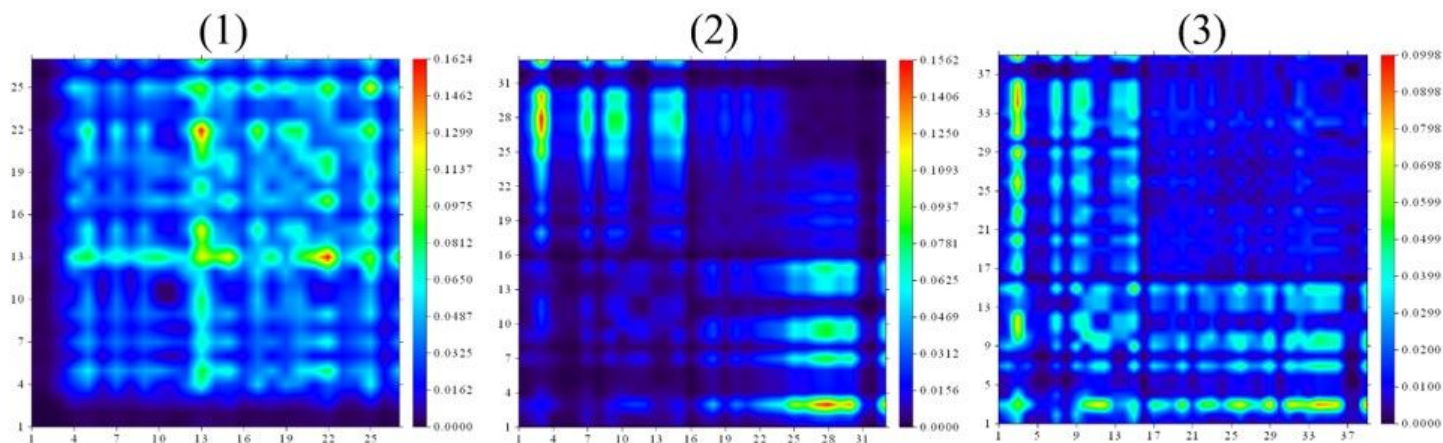
Figure 7

Transition density matrix plots of **(1)** adsorbed PABA+7DMC complex, **(2)** PABA-benzene-7DMC complex, and **(3)** PABA-biphenyl-7DMC complex.
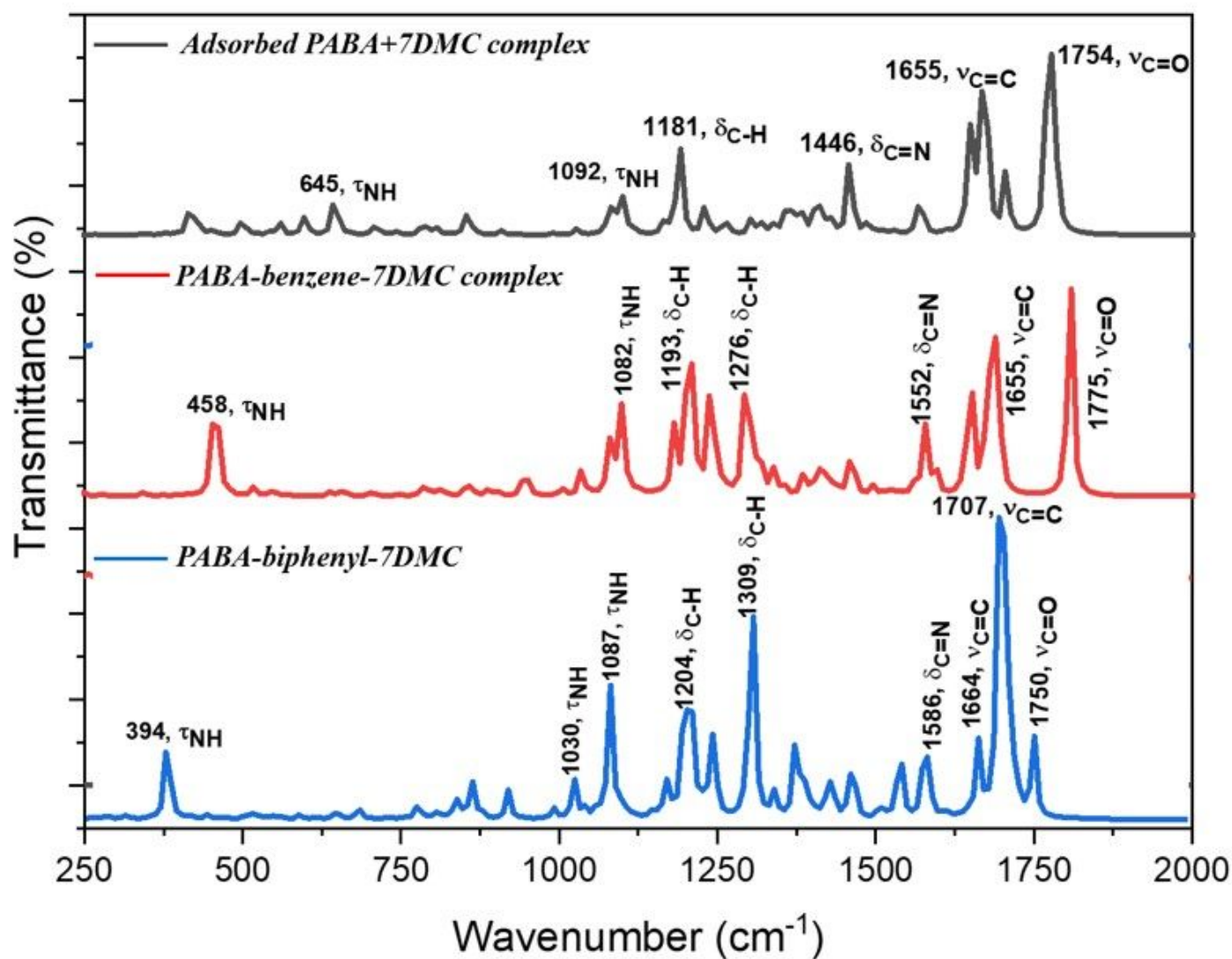
Figure 8

Computed FT-IR spectra of **(1)** adsorbed PABA+7DMC complex, **(2)** PABA-benzene-7DMC complex, and **(3)** PABA-biphenyl-7DMC complex (Symmetric stretching-ν, torsional bending in plane (scissoring)-δ, twisting-τ).
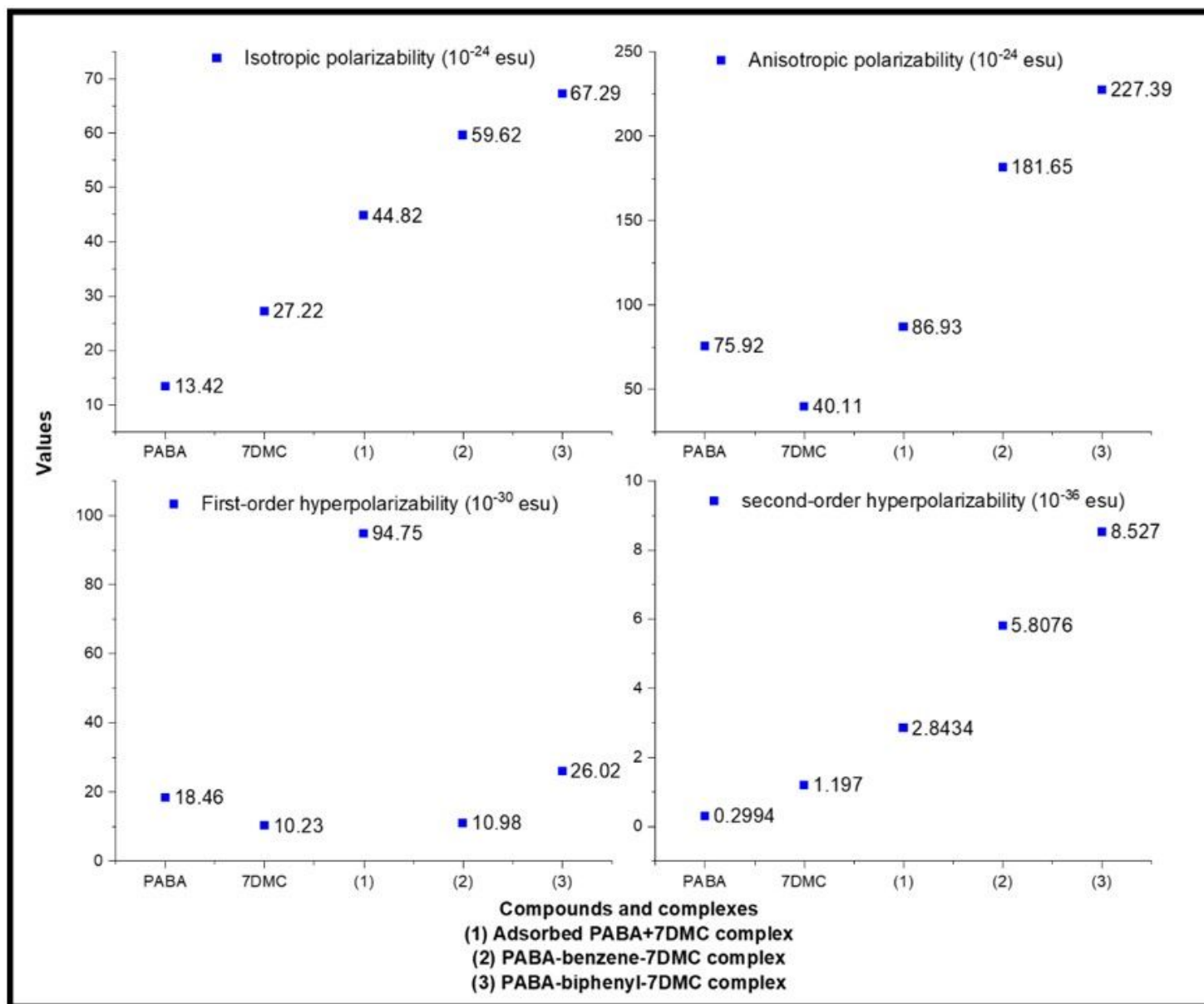

Figure 9

Comparison of the NLO parameters of **(1)** adsorbed PABA+7DMC complex, **(2)** PABA-benzene-7DMC complex, and **(3)** PABA-biphenyl-7DMC complex.

Supplementary Files

This is a list of supplementary files associated with this preprint. Click to download.

- Supportingdocumentd1.docx